

# Early Events During Folding of Wild-type Staphylococcal Nuclease and a Single-tryptophan Variant Studied by Ultrarapid Mixing

Kosuke Maki<sup>1</sup>, Hong Cheng<sup>1</sup>, Dimitry A. Dolgikh<sup>1,2</sup>  
M.C. Ramachandra Shastry<sup>1</sup> and Heinrich Roder<sup>1,3\*</sup>

<sup>1</sup>*Institute for Cancer Research  
Fox Chase Cancer Center  
Philadelphia, PA 19111, USA*

<sup>2</sup>*Shemyakin-Ovchinnikov  
Institute of Bioorganic  
Chemistry, Moscow, 177871  
Russian Federation*

<sup>3</sup>*Department of Biochemistry  
and Biophysics, University of  
Pennsylvania, Philadelphia, PA  
19104-6059, USA*

A continuous-flow mixing device with a dead time of 100  $\mu$ s coupled with intrinsic tryptophan and 1-anilinonaphthalene-8-sulfonate (ANS) fluorescence was used to monitor structure formation during early stages of the folding of staphylococcal nuclease (SNase). A variant with a unique tryptophan fluorophore in the N-terminal  $\beta$ -barrel domain (Trp76 SNase) was obtained by replacing the single Trp140 in wild-type SNase with His in combination with Trp substitution of Phe76. A common background of P47G, P117G and H124L mutations was chosen in order to stabilize the protein and prevent accumulation of *cis* proline isomers under native conditions. In contrast to WT\* SNase, which shows no changes in tryptophan fluorescence prior to the rate-limiting folding step ( $\sim$ 100 ms), the F76W/W140H variant shows additional changes (enhancement) during an early folding phase with a time constant of 75  $\mu$ s. Both proteins exhibit a major increase in ANS fluorescence and identical rates for this early folding event. These findings are consistent with the rapid accumulation of an ensemble of states containing a loosely packed hydrophobic core involving primarily the  $\beta$ -barrel domain while the specific interactions in the  $\alpha$ -helical domain involving Trp140 are formed only during the final stages of folding. The fact that both variants exhibit the same number of kinetic phases with very similar rates confirms that the folding mechanism is not perturbed by the F76W/W140H mutations. However, the Trp at position 76 reports on the rapid formation of a hydrophobic cluster in the N-terminal  $\beta$ -sheet region while the wild-type Trp140 is silent during this early stage of folding. Quantitative modeling of the (un)folding kinetics and thermodynamics of these two proteins *versus* urea concentration revealed that the F76W/W140H mutation selectively destabilizes the native state relative to WT\* SNase while the stability of transient intermediates remains unchanged, leading to accumulation of intermediates under equilibrium conditions at moderate denaturant concentrations.

© 2004 Elsevier Ltd. All rights reserved.

**Keywords:** protein folding kinetics; stopped-flow; continuous-flow; fluorescence; ANS

\*Corresponding author

Present addresses: K. Maki, Department of Physics, Graduate School of Science, University of Tokyo 113-0033, Japan; M. C. R. Shastry, Colgate-Palmolive Company, Piscataway, NJ 08855, USA.

Abbreviations used: ACBP, acyl-CoA binding protein; ANS, 1-anilinonaphthalene-8-sulfonate; Im7, bacterial immunity protein 7; SNase, staphylococcal nuclease; WT\* SNase, P47G/P117/H124L variant of staphylococcal nuclease; Trp76 SNase, F76W/W140H variant of WT\* SNase; CD, circular dichroism.

E-mail address of the corresponding author: heinrich.roder@fcc.edu

## Introduction

Elucidating early events in the transition from the ensemble of unfolded states to the native conformation of a protein is one of the most challenging and critical aspects of the protein folding problem.<sup>1</sup> While some proteins can reach the native state in a single, concerted step,<sup>2</sup> many others fold in stages with significant conformational events occurring within milliseconds of refolding, long before the native population

appears. These structural events are often attributed to accumulation of partially folded intermediates, which may act as stepping stones in finding the unique native conformation.<sup>1,3–5</sup> However, the fact that some (small) proteins fold without detectable intermediates has raised questions concerning the role of intermediates in guiding the polypeptide chain toward its native conformation.<sup>2</sup> In addition, rapid changes observed in folding experiments were suggested to reflect the response of the denatured polypeptide chain to the change in solvent conditions,<sup>6</sup> or they have been dismissed as experimental artifacts.<sup>7</sup> However, advances in rapid mixing techniques<sup>8–11</sup> have made it possible to extend kinetic measurements well into the microsecond time-scale, which enabled us to directly observe some of the previously unresolved (burst-phase) events during folding of a number of proteins.<sup>12–15</sup> The observation of one or more exponential phases preceding the rate-limiting folding step supports the notion that these rapid spectral changes reflect specific barrier-limited folding steps.<sup>16,17</sup>

These studies relied on intrinsic fluorescence from tryptophan (Trp) residues, which can provide information on solvent accessibility, specific tertiary interactions or donor–acceptor distance distributions. Other complementary probes to monitor structure formation, which were successfully combined with ultrarapid mixing devices, are circular dichroism (CD) for monitoring overall secondary structure formation,<sup>18</sup> pulsed hydrogen exchange labeling for monitoring stable hydrogen bonded structures,<sup>19</sup> and small-angle X-ray scattering for monitoring compactness and size of protein molecules.<sup>20,21</sup>

While fluorescence is arguably the most sensitive and versatile spectroscopic probe for folding studies, intrinsic fluorescence from naturally occurring tryptophan residues of some proteins may not be sensitive to early folding events. One such case is the 149 residue protein staphylococcal nuclease (SNase), which contains a single tryptophan residue at position 140 whose fluorescence is substantially enhanced upon folding. However, the fluorescence of Trp140 undergoes little or no change prior to the rate-limiting folding event (~100 ms) despite the fact that significant conformational changes are known to occur at earlier times, based on previous H/<sup>2</sup>H exchange labeling results,<sup>22,23</sup> CD data,<sup>24</sup> and the observation of a lag phase in the appearance of the native structure.<sup>25</sup> The crystal structure of SNase (Figure 1) can be divided into two domains, an N-terminal  $\beta$ -barrel domain consisting of five  $\beta$ -strands (strands I–V) and a C-terminal  $\alpha$ -helical domain consisting of three  $\alpha$ -helices (helix H1–H3).<sup>26</sup> The folding mechanism of SNase has been extensively investigated for more than three decades.<sup>22–25,27,28</sup> Many studies focused on slow folding steps involving *cis*–*trans* isomerization of peptide bonds preceding proline residues<sup>29–31</sup> and heterogeneity of conformations under native conditions arising from proline

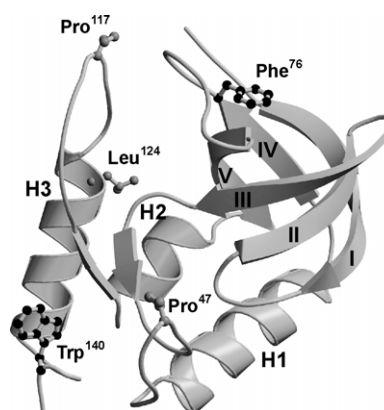


**Figure 1.** Ribbon diagram of H124L SNase based on an NMR structure.<sup>63</sup> Pro47 and Pro117 are replaced by Gly in WT\* SNase. In Trp76 SNase, Phe76 and Trp140 are replaced by Trp and His, respectively, with the background mutations P47G, P117G and H124L. Five  $\beta$ -strands (I–V) and three  $\alpha$ -helices (H1–H3) are explicitly shown. The Figure was prepared using the program MOLSCRIPT.<sup>62</sup>

isomerization.<sup>32–34</sup> SNase also served as an important test case for exploring protein conformation under denaturing conditions.<sup>35,36</sup> Recent pulsed H/<sup>2</sup>H exchange experiments showed that NH groups in the  $\beta$ -barrel domain, especially those in strands II and III, are protected from solvent exchange within ~10 ms of refolding while all other NH probes are protected only during the final stages of folding.<sup>23</sup> However, the fluorescence of the naturally occurring tryptophan residue, Trp140, is insensitive to these early structural events due to its location in the C-terminal region of the protein (Figure 1).

In order to directly observe the formation of the  $\beta$ -barrel domain at an early stage of folding, we constructed an F76W/W140H double mutant of SNase in order to introduce a Trp residue at position 76, a largely buried location at the opening of the  $\beta$ -barrel. Equilibrium studies on several SNase variants containing a Trp in the  $\beta$ -barrel domain have been reported.<sup>37–40</sup> However, the interpretation of these fluorescence studies is complicated by the presence of two Trp residues, which we avoided by replacing the wild-type Trp140 with His (the most stable among a series of substitutions tested; see below). In addition to monitoring the burial of Trp76 due to formation of the hydrophobic core in the  $\beta$ -barrel domain, the development of the hydrophobic core during SNase folding was also observed by monitoring the fluorescence of 1-anilinonaphthalene-8-sulfonate (ANS), a hydrophobic dye known to interact preferentially with loosely packed protein states, including kinetic intermediates.<sup>41</sup> Although ANS can perturb conformational equilibria,<sup>42</sup> and some of the slower kinetic phases may reflect ANS-induced conformational changes,<sup>43</sup> the results

presented below indicate that the initial stages of ANS binding reflect the development of non-polar regions in early compact intermediates.

Both of the single-Trp variants studied here, WT\* SNase and the F76W/W140H double mutant (also denoted Trp76 SNase), contain two Pro to Gly substitutions at positions 47 and 117 designed to eliminate species containing *cis* peptide bonds,<sup>32,44</sup> and the stabilizing H124L mutation.<sup>45</sup> Ultrarapid continuous-flow<sup>11</sup> and conventional stopped-flow techniques were combined to measure the kinetics of folding over the time range from  $\sim 100 \mu\text{s}$  to 100 s, using both intrinsic Trp and extrinsic ANS fluorescence probes. The continuous-flow measurements resolved two faster phases ( $\lambda_1 = 13,500 \text{ s}^{-1}$  and  $\lambda_2 = 3800 \text{ s}^{-1}$ ) in addition to the four slower phases already reported in previous studies<sup>25</sup>. Selective destabilization of the native state of Trp76 SNase resulted in detectable amounts of an equilibrium intermediate at moderate urea concentrations. Quantitative kinetic modeling indicates that all equilibrium and kinetic data for both WT\* and Trp76 SNase can be accounted for by a common kinetic mechanism involving a series of sequential intermediates populated along a major pathway and a minor population folding along a parallel pathway.

## Results

### Construction of the single-tryptophan variant, Trp76 SNase

Because of its location in a largely solvent-shielded position at the C-terminal end of helix H3 (Figure 1), substitution of Trp140 by other aromatic or aliphatic residues may destabilize the native structure of SNase. The thermal unfolding transition of WT\* SNase and four Trp-free variants (W140H, W140F, W140Y and W140L) in the same background as WT\* SNase (P47G/P117G/H124L) was measured by monitoring far-UV CD at 222 nm (in 25 mM sodium phosphate (pH 7.0), 50 mM sodium chloride, 0.5 mM EDTA). All proteins showed cooperative unfolding transitions with midpoint temperatures,  $T_m$ , ranging from 44 °C (W140L) to 66 °C (WT\*). The thermodynamic parameters obtained by non-linear least-squares fitting of a two-state model are listed in Table 1. While all of the tryptophan-free variants are less stable than WT\* SNase, the W140H is the least destabilizing (by 0.4 kcal mol<sup>-1</sup>), and was chosen as a background mutation for the preparation of Trp76 SNase. The thermal unfolding data indicate that replacement of Phe76 by Trp results in an additional 0.6 kcal mol<sup>-1</sup> decrease in stability (Table 1).

### CD spectra of WT\* and Trp76 SNase

In order to detect any structural perturbations due to the tryptophan mutations, Figure 2

**Table 1.** Thermodynamic parameters for thermal unfolding of WT\* SNase, Trp-free variants (W140H, W140F, W140Y, W140L) and Trp76 SNase (F76W/W140H)

	$T_m$ (°C)	$\Delta H$ (kcal mol <sup>-1</sup> )	$\Delta G$ (kcal mol <sup>-1</sup> ) <sup>a</sup>	$\Delta\Delta G$ (kcal mol <sup>-1</sup> ) <sup>a</sup>
WT*	66.3	85.2	6.1	–
W140H	59.0	82.2	5.7	–0.4
W140F	56.9	81.0	5.5	–0.6
W140Y	56.4	76.8	5.0	–1.1
W140L	43.6	42.0	1.6	–4.5
F76W/ W140H	56.6	77.6	5.1	–1.0

All proteins contain the same background substitutions as WT\* SNase (P47G/P117G/H124L). Experimental condition: 25 mM sodium phosphate (pH 7.0), 50 mM NaCl, 0.5 mM EDTA.

<sup>a</sup> Free energy of unfolding at 20 °C.

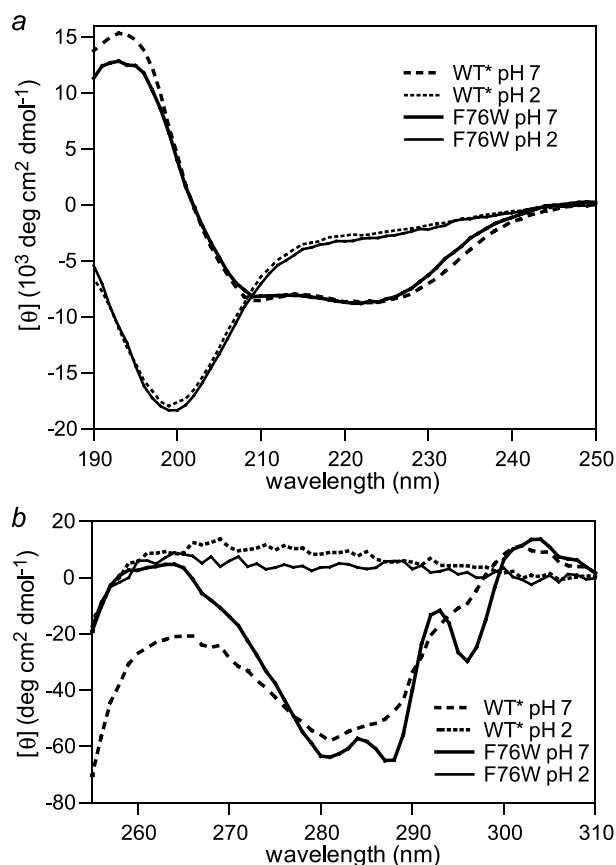


**Figure 2.** CD spectra of WT\* and Trp76 SNase at pH 7.0 as well as 2.0 and 15 °C in (a) far-UV and (b) near-UV regions. The CD spectra of WT\* (broken lines) and Trp76 (continuous lines) SNase at pH 7.0 and 2.0 are shown in thick and thin lines, respectively. The solution contained 20 mM sodium phosphate (pH 7.0) or 10 mM HCl/phosphoric acid (pH 2.0) in addition to appropriate concentrations of the protein. The protein concentrations were 2–10  $\mu\text{M}$  and 50–75  $\mu\text{M}$  for far-UV and near-UV regions, respectively.

compares the CD spectra for WT\* and Trp76 SNase in the far-UV (190–250 nm) and near-UV (250–310 nm) regions under native (20 mM sodium phosphate, pH 7.0) and denaturing (10 mM HCl, 3 mM phosphoric acid, pH 2.0) conditions at 15 °C. The far-UV CD spectrum of Trp76 SNase at pH 7.0 shows a maximum at 193 nm and a broad negative band with two minima at 209 nm and 222 nm, and is very similar to that of WT\* SNase, indicating that the F76W/W140H substitution has a negligible effect on the overall secondary structure. In contrast, the near-UV CD spectra of the two proteins show clear differences at neutral pH. While Trp76 SNase exhibits distinct negative bands at 281.5, 288 and 296.5 nm, these sharp features are broadened out in WT\*, which shows the usual broad aromatic CD band with a minimum at 281 nm and shoulders at 288 and 296 nm. The distinct near-UV CD spectra of these two proteins reflect the different local environments of the two Trp residues. Trp76 appears to be located in a more rigid and anisotropic environment than Trp140, giving rise to a more resolved near-UV CD spectrum. Although the naturally occurring Trp140 is largely buried in the native SNase structure, the Trp side-chain appears to maintain some degree of mobility, consistent with the fact that the C-terminal segment, residues 142–149 is not well defined in the X-ray crystal structure.<sup>26</sup> In contrast, the Trp residue introduced at position 76 is located in a more rigid apolar environment at the edge of the  $\beta$ -barrel domain. The far-UV CD spectra of the two proteins exhibit small but clear differences between 225 nm and 245 nm, which can be explained by differential aromatic contributions in the far-UV region due to the distinct environments of the two tryptophan residues. At pH 2.0, both SNase variants show nearly identical far and near-UV CD spectra characteristic of a fully denatured state devoid of persistent secondary and tertiary structure.

### Equilibrium unfolding of WT\* and Trp76 SNase

Upon excitation at 288 nm, the fluorescence spectra of WT\* and Trp76 SNase at pH 5.2 and 15 °C exhibit emission maxima at 330 and 329 nm, respectively, and yields of 3.4 and 3.6 relative to equimolar *N*-acetyl-L-tryptophanamide (NATA). The substantial blue shift and enhanced emission, compared to NATA ( $\lambda_{\max} = 352$  nm at pH 5.2), indicate that the Trp76 side-chain is largely shielded from the solvent under native conditions. At the same time, the well-resolved near-UV CD spectrum indicates that Trp76 is immobilized within a close-packed environment. At pH 2.0 and 15 °C, the emission maxima and relative yields of these two proteins are close to those of NATA ( $\lambda_{\max} = 351$  nm at pH 2), indicating that the Trp side-chain is solvent-exposed under these denaturing conditions.

The urea-induced unfolding transition of WT\* and Trp76 SNase was measured by recording a

series of fluorescence emission spectra,  $Em(\lambda)$ , over the range from 300 nm to 450 nm (with excitation at 288 nm) at urea concentrations,  $c$ , ranging from 0 M to 7.5 M. All spectra for a given protein were recorded in one session, using a computer-controlled syringe titrator, which makes it possible to use global fitting methods for data analysis. For global fitting, the original data set,  $Em(\lambda)$  at various denaturant concentrations, was transposed, yielding a set of unfolding transition curves,  $Em(c)$ , at different wavelengths (representative examples at selected wavelengths are shown in Figure 3a and b). Non-linear least-squares fitting of two-state or three-state equilibrium models, using a global fitting algorithm (see Materials and Methods) yielded a set of global parameters (mid-point concentrations,  $C_m$ , and  $m$ -values for each transition) and local parameters (intercepts and slopes for the native and unfolded baselines, respectively, at each wavelength). The unfolding transition of WT\* SNase is well fitted by using a two-state model (Figure 3a). However, in the case of Trp76 SNase, two-state analysis resulted in a noticeably lower quality of the fits ( $\chi^2 = 0.0071$ ), especially between 2 M and 3 M urea (Figure 4, inset). Global fitting of a three-state model consisting of native ( $N$ ), intermediate ( $I_{eq}$ ) and unfolded ( $U_{eq}$ ) states to the combined data for Trp76 SNase (Figure 3b) resulted in a nearly twofold decrease in  $\chi^2$  (0.0039). In addition, the three-state model yielded somewhat smaller residuals than the two-state model (Figure 4). The global (thermodynamic) parameters thus obtained are listed in Table 2. Based on these equilibrium parameters, the population of each species can be calculated as a function of urea concentration (continuous lines in Figure 3c and d). The F76W/W140H mutations destabilize the native structure by about 2.5 kcal mol<sup>-1</sup> and result in a substantial population of an equilibrium intermediate (~50% at 2 M urea).

The fitting of the transition curves at each wavelength gives a collection of fluorescence intensities of each species linearly extrapolated to 0 M urea over the range of wavelengths (Figure 3e and f). The extrapolated fluorescence spectra for  $N$  are identical with those observed at 0 M urea with  $\lambda_{\max}$  near 330 nm and three- to fourfold enhanced fluorescence yield compared to the unfolded state (or NATA). The extrapolated fluorescence spectra for the  $U$ -state exhibit virtually no wavelength shift and only slightly lower intensity than those measured directly in 7.5 M urea, indicating that the environments around the Trp residues of unfolded WT\* and Trp76 SNase are insensitive to urea concentration (the lower intensity of the extrapolated spectra is expected from the positive slope of the curves in the unfolding region). The fluorescence spectrum of  $I_{eq}$  for Trp76 SNase at 0 M urea has slightly higher intensity than that of  $U_{eq}$  with a 6 nm blue shift, indicating that Trp76 in this intermediate state is somewhat more buried than in the fully unfolded state. Although the fluorescence properties of intermediate and

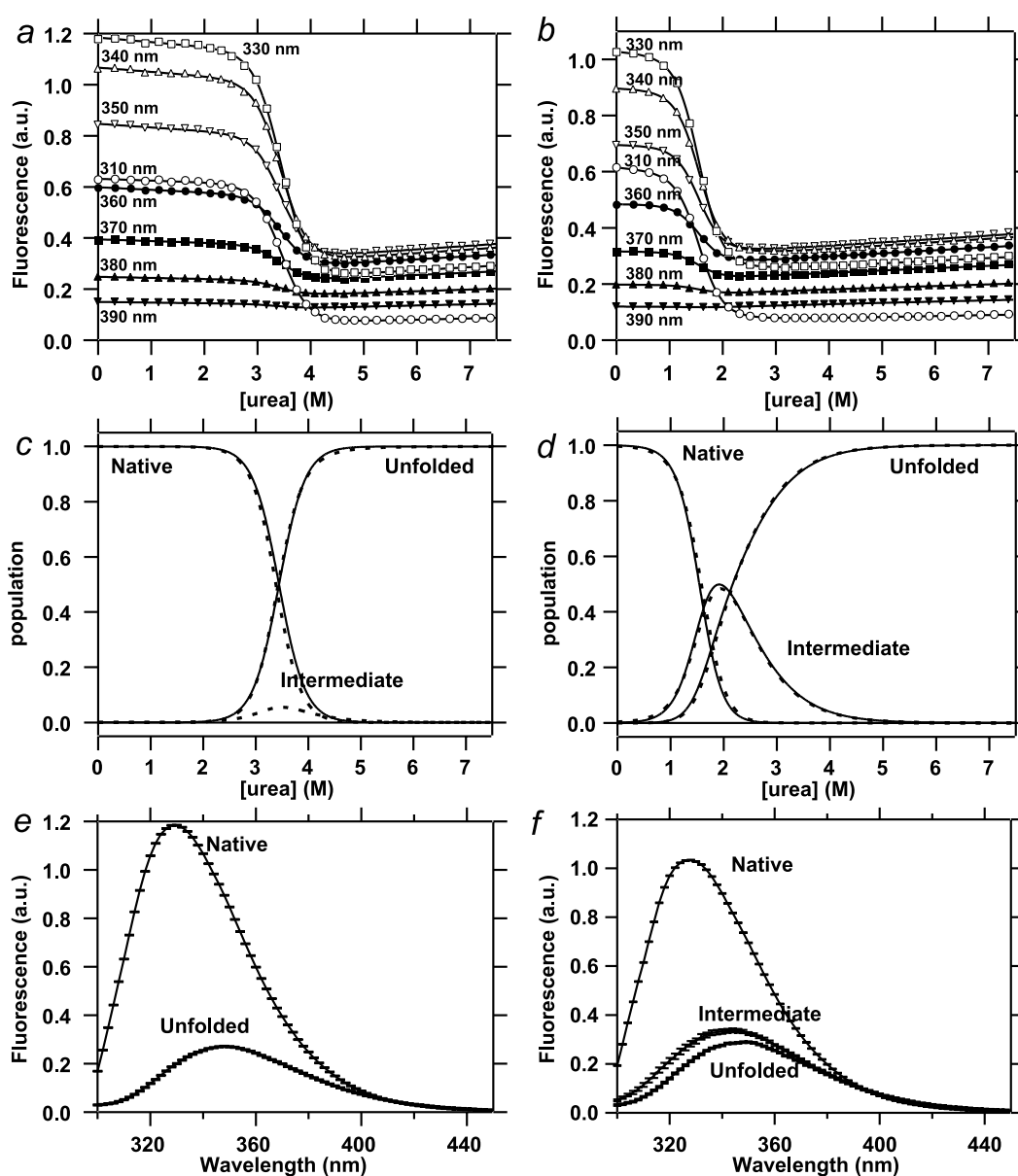


**Figure 3.** Urea-induced equilibrium unfolding transition monitored by tryptophan fluorescence spectroscopy. The top panels show unfolding transition curves of WT\* SNase (a) and Trp76 SNase (b) at representative wavelengths versus urea concentration. Continuous lines are predicted curves obtained by fitting the data globally, based on two-state (WT\*) or three-state (Trp76) models. The middle panels show the populations of native (N), intermediate ( $I_{eq}$ ) and unfolded ( $U_{eq}$ ) states of WT\* SNase (c) and Trp76 SNase (d) as a function of urea concentration predicted on the basis of equilibrium (continuous lines) or kinetic (broken lines) experiments. For kinetically predicted populations, based on Scheme 4,  $I_{eq}$  represents the combined populations of the  $I_2$  and  $I'$  states and U includes the U and  $U'$  states (state M has negligible population under all conditions). The bottom panels show the deconvoluted fluorescence spectra of the N,  $I_{eq}$  and  $U_{eq}$  states of WT\* SNase (e) and Trp76 SNase (f) in the absence of urea predicted by global fitting of two-state (WT\*) or three-state (Trp76) models to the equilibrium unfolding data.

unfolded states are similar, the spectra are clearly distinct as indicated by the error bars in Figure 3f, which are based on the standard deviation of the corresponding parameter in the global fitting procedure.

We also followed the unfolding transition of Trp76 SNase by monitoring the changes in the far-UV CD spectrum at 222 nm (Figure 4b). An excellent fit was obtained by using the thermodynamic parameters derived from the global

three-state analysis of the fluorescence spectra (continuous lines; an unconstrained three-state fit results in a virtually indistinguishable transition). In contrast, a two-state model led to systematic deviations (broken lines), especially at urea concentrations between 2.5 M and 5 M (inset). As in the case of the fluorescence data (Figure 4a), the global three-state parameters also yielded smaller residuals (upper panel in Figure 4b) and a nearly twofold improvement in  $\chi^2$  (0.7 versus 1.3). The

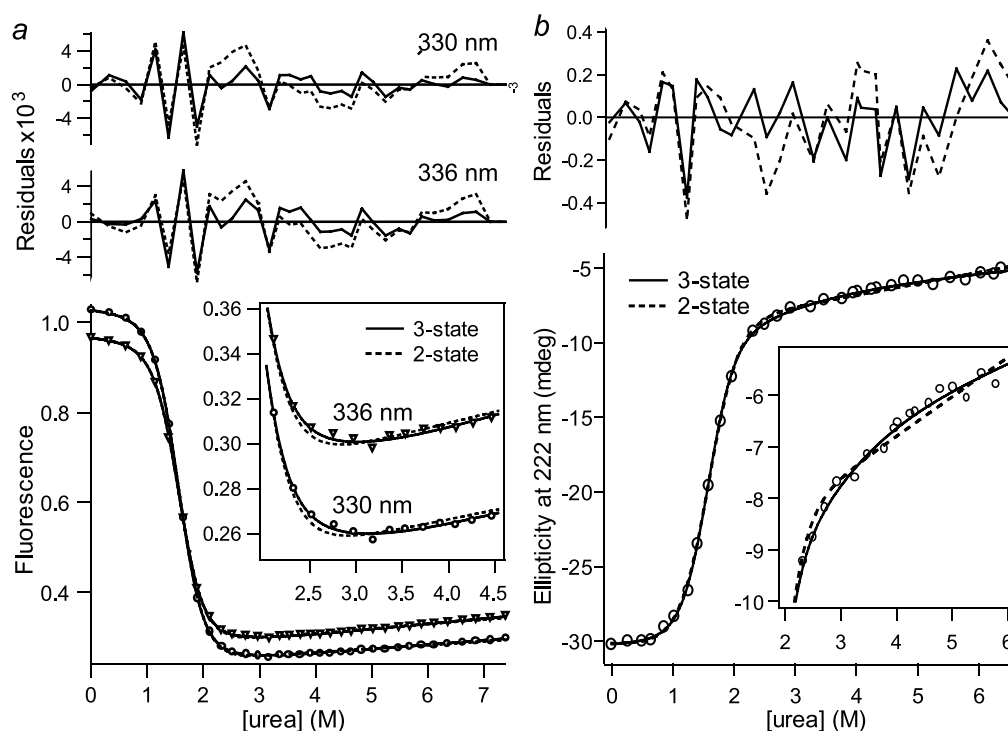


**Figure 4.** Comparison of three-state (continuous lines) and two-state (broken lines) equilibrium fits to the unfolding transitions of Trp76 SNase monitored by fluorescence emission at 330 and 336 nm (a) and the CD signal at 222 nm (b), along with residuals (upper panels). The insets in each panel show expanded plots of the post-transition regions where the improvement of the three-state model is especially pronounced. The continuous line in b represents a constrained fit of a three-state transition to the CD data using the thermodynamic parameters ( $C_{m1} = 1.63$  M,  $m_1 = 2.4$  kcal mol<sup>-1</sup> M<sup>-1</sup>,  $C_{m2} = 2.1$  M,  $m_2 = 0.9$  kcal mol<sup>-1</sup> M<sup>-1</sup>) obtained by global fitting of the combined fluorescence data (Figure 3). An unconstrained fit resulted in very similar parameters ( $C_{m1} = 1.66$  M,  $m_1 = 2.4$  kcal mol<sup>-1</sup> M<sup>-1</sup>,  $C_{m2} = 2.1$  M,  $m_2 = 0.7$  kcal mol<sup>-1</sup> M<sup>-1</sup>) and an indistinguishable unfolding curve.

relative CD signals for the  $N$ ,  $I_{eq}$  and  $U_{eq}$  states obtained in this fit indicate that the equilibrium intermediate contains about 15% residual  $\alpha$ -helical structure. The three-state equilibrium unfolding mechanism for Trp76 SNase is further supported by the kinetic data described below; the urea-

dependent populations of native, intermediate and unfolded states predicted by the kinetic model (broken lines in Figure 3d) are in quantitative agreement with those obtained by global analysis the equilibrium fluorescence data (continuous lines).

**Table 2.** Thermodynamic parameters describing the urea-dependent equilibrium unfolding transitions of WT\* and Trp76 SNase

	WT* SNase		Trp76 SNase	
	Equilibrium <sup>a</sup>	Kinetic <sup>b</sup>	Equilibrium <sup>a</sup>	Kinetic <sup>b</sup>
$C_{mUN}$ (M)	$3.45 \pm 0.01$	3.41	n. a.	n. a.
$m_{UN}$ (kcal mol <sup>-1</sup> M <sup>-1</sup> )	$2.30 \pm 0.01$	2.50	$3.36^c$	3.29
$\Delta G_{UN}^{H_2O}$ (kcal mol <sup>-1</sup> )	$7.92 \pm 0.02$	8.53	$5.98^c$	5.93
$C_{mU_{eq}}$ (M)	–	2.15	$2.12 \pm 0.27$	2.12
$m_{U_{eq}}$ (kcal mol <sup>-1</sup> M <sup>-1</sup> )	–	0.97	$0.96 \pm 0.18$	0.97
$\Delta G_{U_{eq}}^{H_2O}$ (kcal mol <sup>-1</sup> )	–	2.09	$2.08 \pm 0.63$	2.05
$C_{m_{eqN}}$ (M)	–	4.21	$1.63 \pm 0.04$	1.67
$m_{eqN}$ (kcal mol <sup>-1</sup> M <sup>-1</sup> )	–	1.53	$2.40 \pm 0.08$	2.32
$\Delta G_{eqN}^{H_2O}$ (kcal mol <sup>-1</sup> )	–	6.43	$3.90 \pm 0.23$	3.88

Experimental conditions: 100 mM sodium acetate at pH 5.2 and 15 °C.

<sup>a</sup> Thermodynamic parameters obtained by fitting two-state or three-state models to fluorescence-detected equilibrium unfolding data. Error estimates for equilibrium parameters are based on goodness of fit ( $\pm$  one standard deviation).

<sup>b</sup> Thermodynamic parameters calculated from the microscopic rate constants and kinetic  $m$ -values (Table 5) estimated by kinetic modeling (see Materials and Methods).

<sup>c</sup>  $\Delta G_{UN}^{H_2O}$  and  $m_{UN}$  were calculated by adding the corresponding thermodynamic parameters for  $U \leftrightarrow I$  and  $I \leftrightarrow N$  transitions.

To confirm that the unfolding transition of Trp76 SNase is fully reversible, we compared the CD spectra of two Trp76 SNase solutions under matching native conditions (at a low urea concentration). One solution was prepared by dissolving lyophilized Trp76 SNase into a buffer containing 0.63 M urea and 20 mM sodium phosphate (pH 7.0) while the other was obtained by tenfold dilution of an unfolded Trp76 SNase solution containing 6.26 M urea with 20 mM sodium phosphate (pH 7.0). The far-UV CD spectra of these two protein solutions were indistinguishable (data not shown). This rules out the possibility that accumulation of an equilibrium intermediate is caused by an irreversible process, such as aggregation.

### Folding kinetics of WT\* and Trp76 SNase monitored by intrinsic Trp fluorescence

The folding kinetics of WT\* and Trp76 SNase were monitored with the Trp fluorescence by continuous-flow and stopped-flow measurements, following a pH jump from the acid-unfolded state (pH 2.0) to pH 5.2 at 15 °C (see Materials and Methods). As shown in Figure 5a, the kinetic traces from continuous-flow and stopped-flow measurements cover the time window from 100  $\mu$ s to 10 s after initiating refolding (dead times of the continuous-flow and stopped-flow measurements were 100  $\mu$ s and 2.4 ms, respectively). The kinetic traces are fitted to a sum of four and six exponential functions for WT\* and Trp76 SNase, respectively. Kinetic parameters thus obtained are listed in Table 3.

The rates and amplitudes of the slower four phases detected by stopped-flow measurements show trends very similar to those observed in a previous study.<sup>25</sup> The slowest phase (phase 6;  $\lambda_6 \sim 0.01 \text{ s}^{-1}$ ) reflects a small fraction of molecules whose folding is rate-limited by proline isomerization,<sup>29</sup> which will not be further considered here. Phase 4 ( $\lambda_4 \sim 10 \text{ s}^{-1}$ ) is the dominant phase during refolding of these two proteins and corresponds to the rate-limiting step during folding for the majority of molecules folding along the predominant folding pathway, and phase 5 ( $\lambda_5 \sim 1 \text{ s}^{-1}$ ) is assigned to the rate-limiting step for a smaller population of molecules following a parallel folding pathway. A lag phase (phase 3;  $\lambda_3 \sim 70 \text{ s}^{-1}$ ) was also found in previous studies of several SNase variants.<sup>25,31</sup> In addition to these four phases, continuous-flow measurements showed two additional fast phases (phase 1,

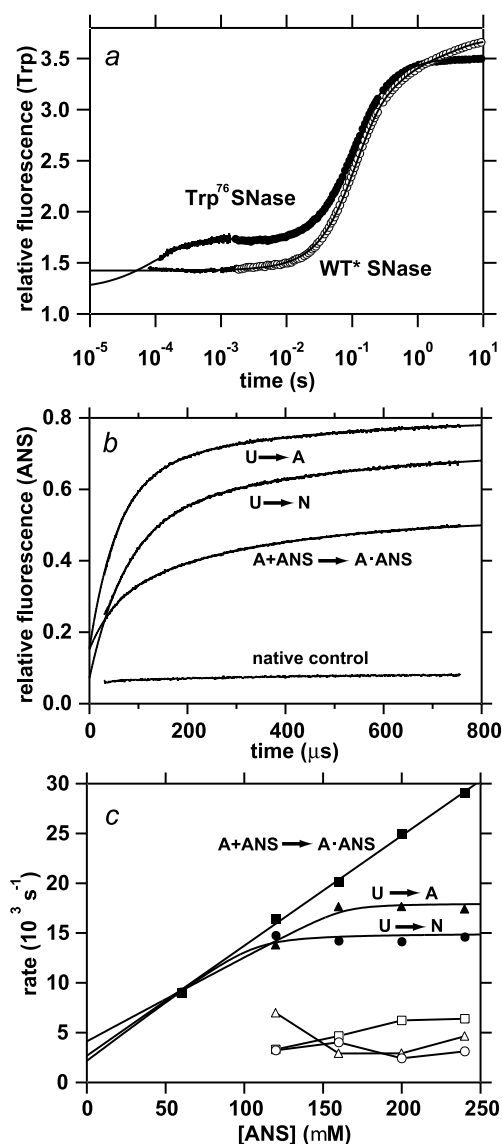


**Figure 5.** *a*, Refolding kinetics of WT\* and Trp76 SNase induced by a pH-jump from 2.0 to 5.2 measured by continuous-flow fluorescence at 15 °C. *b*, ANS fluorescence changes during binding/folding reactions of Trp76 SNase measured by continuous-flow experiments in the presence of 160  $\mu$ M ANS at 15 °C. U  $\rightarrow$  A, salt concentration jump from 0 M to 1 M KCl at pH 2.0; U  $\rightarrow$  N, refolding induced by a pH jump from 2.0 to 5.2; A + ANS  $\rightarrow$  A·ANS, ANS binding kinetics in the presence of 1 M KCl at pH 2.0; native control, ANS binding kinetics under the native conditions (pH 5.2). *c*, ANS concentration dependence of the rates for the fast (filled symbols) and slow (open symbols) phases observed during the U  $\rightarrow$  A ( $\blacktriangle$ ), U  $\rightarrow$  N ( $\bullet$ ), and A + ANS  $\rightarrow$  A·ANS ( $\blacksquare$ ) reactions.

**Table 3.** Apparent rate constants and relative amplitudes of pH-induced folding of WT\* and Trp76 SNase

	$A_1$	$\lambda_1 \text{ (s}^{-1}\text{)}$	$A_2$	$\lambda_2 \text{ (s}^{-1}\text{)}$	$A_3$	$\lambda_3 \text{ (s}^{-1}\text{)}$	$A_4$	$\lambda_4 \text{ (s}^{-1}\text{)}$	$A_5$	$\lambda_5 \text{ (s}^{-1}\text{)}$	$A_6$	$\lambda_6 \text{ (s}^{-1}\text{)}$
WT* SNase	–	–	–	–	0.23	40.6	–1.78	10.4	–0.40	1.35	–0.26	0.10
Trp76 SNase	–0.31	13525	–0.19	3873	0.32	41.3	–1.51	11.3	–0.43	2.3	–0.24	0.01

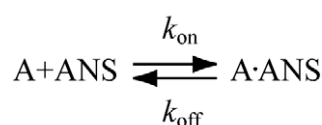
Rate constants and amplitudes of the kinetic phases observed in pH-induced continuous-flow and stopped-flow fluorescence experiments. Refolding conditions: 0.1 M sodium acetate buffer at pH 5.2 and 15 °C.

$\lambda_1 = \sim 12,000 \text{ s}^{-1}$ ; and phase 2,  $\lambda_2 = \sim 4000 \text{ s}^{-1}$ ) with increasing fluorescence only during refolding of Trp76 SNase, indicating that Trp76 is partially buried already during the early stages of the folding. In contrast, no detectable change in fluorescence was observed for WT\* SNase within the first millisecond of refolding, indicating that on this time-scale the environment of Trp140 remains virtually unchanged. The initial fluorescence intensity of approximately 1.3–1.4 relative to the acid-unfolded state at pH 2.0 (Figure 5a) does not necessarily mean the formation of a burst-phase intermediate within the dead time of the continuous-flow measurements. The fluorescence of NATA, which is a good model for the solvent-exposed Trp side-chain in the unfolded state, is approximately 1.3-fold more intense at pH 5.2 than that at pH 2.0 at 15 °C (data not shown), and thus accounts for the observed fluorescence intensity at early folding times, both for WT\* and Trp76 SNase.

### ANS as a probe to monitor the early stages of folding

ANS has often been used as a structural probe in folding studies, taking advantage of the large amplification of its fluorescence on binding to hydrophobic surfaces or clusters,<sup>41</sup> which is one of the characteristics of transient folding intermediates and partially structured equilibrium intermediates, such as the salt-induced collapsed states observed under acidic conditions (A-state). Although it is assumed that the preferential binding of ANS during folding is so fast that the binding process itself does not perturb refolding reactions under typical experimental conditions, it remains unclear what actually occurs during early stages of folding in the presence of ANS. Thus, our first aim was to understand the mechanism underlying ANS binding during the refolding of WT\* and Trp76 SNase using continuous-flow mixing. Figure 5b shows kinetic traces of Trp76 SNase on pH-induced refolding from the acid-unfolded state at pH 2.0 to native conditions (at pH 5.2) and high salt conditions (1.0 M KCl at pH 2.0), where SNase preferentially forms the A-state. Also shown is the kinetics of ANS binding to the A-state, which serves as a reference binding reaction not involving refolding. Experiments were carried out at 15 °C in the presence of 160  $\mu\text{M}$  ANS, whose fluorescence was monitored above 418 nm upon excitation at 366 nm. Compared with tryptophan, the sensitivity of ANS fluorescence is much higher, so that the quality of the continuous-flow data was excellent even at relatively low protein concentrations ( $\sim 5 \mu\text{M}$ ).

The kinetic traces could be well fitted to double-exponential functions with little or no missing amplitudes (Figure 5b), indicating that the observed time window accounts for the complete ANS-detected reaction. Figure 5c shows the ANS concentration dependence of the apparent ANS-



Scheme 1.



Scheme 2.

binding rates observed under different reaction conditions (formation of the A-state, refolding to the native state, and ANS binding to the preformed A-state). The rate of the faster one of the two kinetic phases observed varies linearly with ANS concentration, and can be modeled as a simple pseudo-first-order reaction (Scheme 1), where  $k_{\text{on}}$  and  $k_{\text{off}}$  represent association and dissociation rate constants (see Materials and Methods). The rate of the major (faster) phase observed in refolding experiments ( $\text{U} \rightarrow \text{A}$  or  $\text{U} \rightarrow \text{N}$ ) shows a linear increase at low ANS concentration, followed by saturation at higher ANS concentrations ( $\geq 120 \mu\text{M}$ ), which is accounted for by an extended version of Scheme 1 (Scheme 2), where  $\text{I}_{\text{acc}}$  represents an ensemble of compact folding intermediates able to associate with ANS.  $k_{\text{U}_{\text{I}_{\text{acc}}}}$  and  $k_{\text{I}_{\text{acc}}\text{U}}$  represent the microscopic rate constants of interconversion between U and  $\text{I}_{\text{acc}}$  (see Materials and Methods). The continuous lines in Figure 5c represent the ANS concentration dependence of the apparent rates obtained by quantitative modeling based on Schemes 1 and 2. The kinetic parameters used in the modeling are given in Table 4. The equilibrium dissociation constant  $K_{\text{d}} = k_{\text{off}}/k_{\text{on}} = 24 \mu\text{M}$  is consistent with corresponding dissociation constant obtained in an

**Table 4.** Kinetic parameters of Trp76 SNase estimated by modeling the kinetics of ANS binding to the A-state, and the changes in ANS fluorescence during refolding under native or A-state conditions

Reaction	$k_{\text{on}}$ ( $\text{s}^{-1} \mu\text{M}^{-1}$ )	$k_{\text{off}}$ ( $\text{s}^{-1}$ )	$k_{\text{U}_{\text{I}_{\text{acc}}}}$ ( $\text{s}^{-1}$ )	$k_{\text{I}_{\text{acc}}\text{U}}$ ( $\text{s}^{-1}$ )
$\text{A} + \text{ANS} \leftrightarrow \text{A} \cdot \text{ANS}^{\text{a}}$	110	2680	–	–
$\text{U} \leftrightarrow \text{N} (+ \text{ANS})^{\text{b}}$	120	2000	15,000	200
$\text{U} \leftrightarrow \text{A} (+ \text{ANS})^{\text{c}}$	85	4000	18,000	50

<sup>a</sup> ANS binding kinetics to the A-state at 15 °C. Experimental conditions: 20 mM phosphoric acid, 1 M KCl (pH 2.0).

<sup>b</sup> Refolding kinetics from the acid-unfolded state to native conditions at 15 °C. Refolding conditions: 100 mM sodium acetate (pH 5.3).

<sup>c</sup> Refolding kinetics from acid-unfolded state to high salt concentration at 15 °C. Refolding conditions: 20 mM phosphoric acid, 1 M KCl (pH 2.0).

equilibrium titration experiment of ANS binding to the A-state (93  $\mu\text{M}$ , data not shown). Below  $\sim 100 \mu\text{M}$  ANS the apparent rate observed under folding conditions is linearly dependent on ANS concentration, approaching the pseudo-first-order behavior of ANS binding to the A-state. Thus, under all reaction conditions, ANS binding is rate limiting at low ANS concentration. In contrast, above  $\sim 120 \mu\text{M}$  ANS, the apparent rate constants level off (Figure 5c), indicating that the reaction is no longer pseudo-first-order, but is rate-limited by a unimolecular process. The limiting rates ( $1.4 \times 10^4 \text{ s}^{-1}$  and  $1.75 \times 10^4 \text{ s}^{-1}$  for the  $\text{U} \rightarrow \text{N}$  and  $\text{U} \rightarrow \text{A}$  reactions, respectively) are in excellent agreement with the apparent rate constants of the fastest phase (phase 1) in the pH-induced refolding reaction of Trp76 SNase monitored by Trp fluorescence ( $1.35 \times 10^4 \text{ s}^{-1}$ ), confirming that early conformational events in folding are the rate-determining step for ANS binding.

The apparent rate constant of the slower phase (phase 2) observed in the ANS binding experiments,  $\sim 4000 \text{ s}^{-1}$  independent of ANS concentration, is similar to the rate of the second phase in the folding kinetics monitored by intrinsic fluorescence ( $\lambda_2 = 3870 \text{ s}^{-1}$ ; Table 3). Therefore, phase 2 also reflects an intramolecular conformational event. The fact that intrinsic tryptophan fluorescence and the extrinsic ANS probe yield the same rates for the first two folding phases provides clear evidence that ANS binding does not perturb the kinetics of conformational transitions on the submillisecond time-scale. The similarity of the kinetic behavior between refolding reactions to the A and N states (Figure 5c) indicates that a common early step occurs in the formation of the A state and the pH-induced folding reaction, despite significantly different final conditions (20 mM phosphoric acid and 1.0 M KCl, pH 2.0 versus  $\sim 100 \text{ mM}$  sodium acetate, pH 5.2). Finally, we performed a matching series of continuous-flow measurements of ANS binding during refolding and A-state formation of WT\* SNase (data not shown). The rates and amplitudes obtained are very similar to those of Trp76 SNase (Table 4), indicating that the early stages are not significantly perturbed by the amino acid changes involved (F76W and W140H).

#### Urea concentration dependence of folding and unfolding kinetics of WT\* and Trp76 SNase

The refolding kinetics of WT\* and Trp76 SNase were measured by monitoring ANS fluorescence at various urea concentrations ranging from 0.44 M to 2.78 M at pH 5.2 and 15  $^\circ\text{C}$ , using the continuous-flow method. Representative kinetic traces of WT\* and Trp76 SNase are shown in Figure 6a and b, respectively. Each kinetic trace was fit by a double (0.44–1.89 M urea) or a single-exponential function (2.27–2.78 M urea). The close similarity of the kinetic traces for WT\* and Trp76 SNase (Figure 6) further supports our conclusion

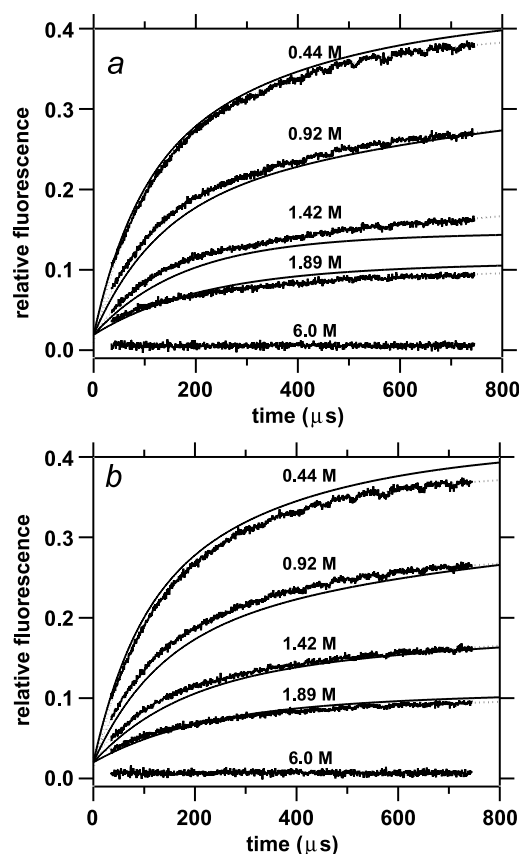


**Figure 6.** Refolding kinetics of (a) WT\* and (b) Trp76 SNase following a urea concentration jump measured by continuous-flow experiments in the presence of 160  $\mu\text{M}$  ANS at pH 5.2 and 15  $^\circ\text{C}$ . Final urea concentrations are shown above each kinetic trace. The fluorescence intensity was scaled relative to the ANS fluorescence in the presence of the protein of matching concentration and 1 M KCl at pH 2.0.

that both proteins experience a common early step in the refolding reaction.

Urea concentration dependence of the folding and unfolding kinetics of WT\* and Trp76 SNase were also measured in stopped-flow experiments by monitoring Trp fluorescence under experimental conditions matching those of the continuous-flow measurements (pH 5.2, 15  $^\circ\text{C}$ , excitation wavelength 288 nm). The observed rates are plotted in Figure 7 as a function of urea concentration. Apart from the fastest two phases described above, the folding of these two proteins consists of four phases at lower urea concentrations while two or three phases are observed at higher urea concentrations. The lag phase (phase 3) accelerates with increasing urea concentration before it disappears around 1 M urea. As pointed out in previous studies,<sup>25,31</sup> phase 3 is remarkable in that the amplitude has a sign opposite to the other phases, which indicates accumulation of an intermediate with fluorescence properties similar to U. Phase 4 of WT\* SNase (Figure 7a) is the dominant phase at 0.3 M urea ( $\sim 70\%$  of the amplitude), and its rate constant,  $\lambda_4$ , is highly sensitive to

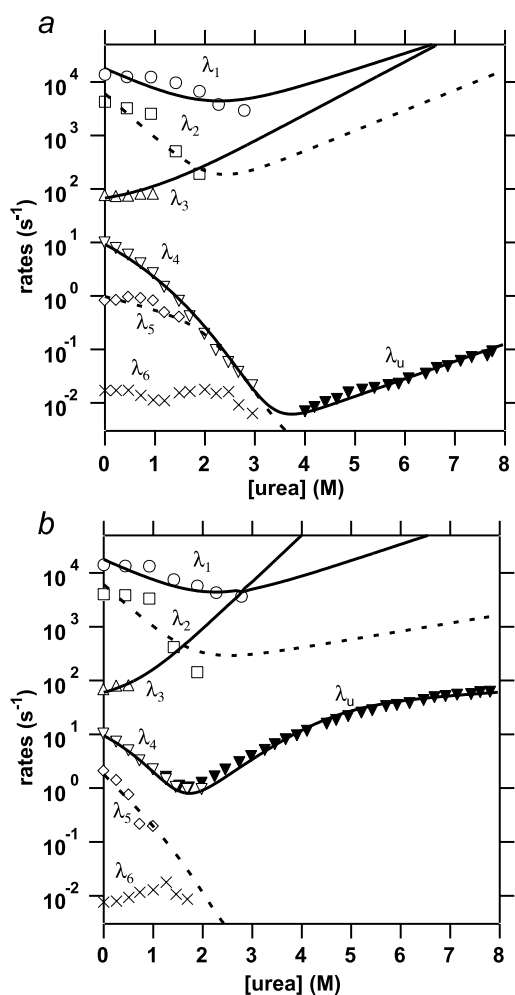


**Figure 7.** Urea concentration dependence of the rates of refolding (open symbols and cross) and unfolding (filled symbols) of WT\* (a) and Trp76 SNase (b) measured in continuous-flow and stopped-flow experiments under matching conditions ( $\sim 100$  mM sodium acetate, pH 5.2, 15 °C). The two fastest refolding phases,  $\lambda_1$  and  $\lambda_2$  were measured by continuous-flow ANS fluorescence while the slower refolding phases,  $\lambda_3$ – $\lambda_6$ , as well as the single unfolding phase ( $\blacktriangledown$ ) were measured by stopped-flow fluorescence. The rate constants predicted by Scheme 4 (see the text) are shown as continuous lines (major folding channel,  $U \leftrightarrow I_1 \leftrightarrow I_2 \leftrightarrow M \leftrightarrow N$ ) and broken lines (minor folding channel ( $U' \leftrightarrow I' \leftrightarrow M \leftrightarrow N$ )).

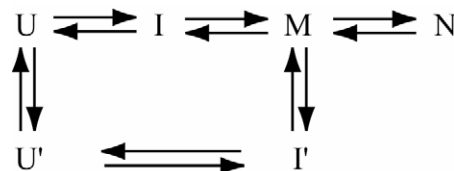
denaturant, decreasing from about  $10 \text{ s}^{-1}$  at 0.3 M urea to  $\sim 0.1 \text{ s}^{-1}$  at 3.5 M urea (the midpoint of the unfolding transition). In the case of Trp76 SNase (Figure 7b),  $\lambda_4$  traces that of WT\* SNase until reaching its minimum at around 1.5 M urea, consistent with its decreased stability compared to WT\* SNase. The rate constant of phase 5 of both proteins ( $\lambda_5$ ) also decreases monotonically with increasing urea concentration.

The unfolding kinetics of WT\* and Trp76 SNase are well described by single-exponential functions by virtue of the replacement of Pro117 by glycine, which prevents formation of a heterogeneous population of the native state.<sup>29</sup> The unfolding rate,  $\lambda_u$ , approaches  $\lambda_4$  in the transition region,

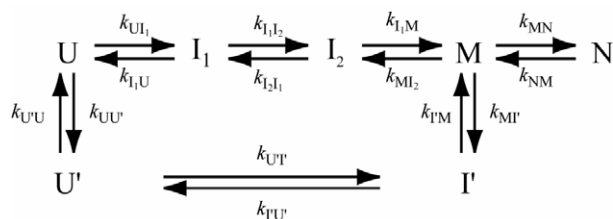
indicating that this is the rate-determining phase in the overall folding–unfolding transition. The unfolding limb of Trp76 SNase shows pronounced curvature, which is explained by the presence of a native-like intermediate, M, which gives rise to a denaturant-dependent switch in the rate-limiting barriers encountered during unfolding. At high urea concentrations, the transition from N to M, which depends only mildly on denaturant concentrations, limits the rate of unfolding while at lower urea concentrations the unfolding step from M with its strongly urea-dependent rate constant determines the unfolding kinetics. However, the curvature in the unfolding limb of WT\* SNase is less pronounced because the accessible range of urea concentrations is insufficient to reach the regime where the  $N \rightarrow M$  transition is rate-limiting (see below).

### Quantitative modeling of the folding kinetics of WT\* and Trp76 SNase

Walkenhorst *et al.* proposed a five-state kinetic scheme (Scheme 3) in their study on H124L SNase and a proline-free variant,<sup>25</sup> where I and M are intermediate ensembles on the major folding pathway, explaining the curvature found in the folding limb of phase 4 and unfolding limbs, respectively, while U' and I' are the unfolded and the intermediate states populated along a minor parallel folding pathway. I' is required to account for the minor phase with a rate slower than  $\lambda_4$  ( $\lambda_5$ ). Our continuous-flow measurements revealed two additional faster phases (phase 1 and phase 2), which can be accounted for by an extended scheme (Scheme 4), where  $I_2$  corresponds to I in Scheme 3, and  $I_1$  and I' are intermediates responsible for phases 1 and 2, respectively (see below). The microscopic rate constants,  $k_{ij}$ , are defined by equation (2) (see Materials and Methods). The rate constant in the absence of denaturant,  $k_{ij}^0$ , and the



Scheme 3.



Scheme 4.

denaturant dependence of the microscopic rate constants,  $m_{ij}^\ddagger$ , were varied to reproduce the urea concentration dependence of the folding/unfolding rates and amplitudes as well as equilibrium properties, based on Scheme 4. The predicted rates for folding along the major and minor pathways are shown in Figure 7 as continuous and broken lines, respectively.

We first focus on the behavior of phases 1 and 2 because these faster phases are not significantly coupled with the four slower phases. Each phase represents accumulation of intermediates on either folding pathway. If they represented a series of intermediates on the same folding pathway, at least one additional faster phase is needed to account for the  $U(i) \leftrightarrow I(i)$  step on the other folding pathway. However, we were unable to detect any missing amplitude in the kinetic traces monitored by both Trp and ANS fluorescence, arguing against an additional phase. To account for the kinetic data, one additional intermediate ( $I_1$ ) is required to be placed on the major pathway while no additional intermediate is required on the minor pathway. For Trp76 SNase, the observation of a cooperative transition between  $U_{eq}$  and  $I_{eq}$  obtained by equilibrium unfolding experiments requires that phases 1 and 2 are located on the major and minor pathway, respectively, because the equilibrium  $m$ -value for the  $U_{eq} \leftrightarrow I_{eq}$  transition,  $m_{U_{eq}}$ , which primarily reflects the major pathway, is  $0.96 \text{ kcal mol}^{-1} \text{ M}^{-1}$ , which is better approximated by the kinetic  $m$ -values for phase 1 ( $m_{IU}^\ddagger - m_{UI}^\ddagger = 0.96 \text{ kcal mol}^{-1} \text{ M}^{-1}$ ) than that of phase 2 ( $m_{I'U'}^\ddagger - m_{U'I'}^\ddagger = 1.30 \text{ kcal mol}^{-1} \text{ M}^{-1}$ ). If we were to assign  $\lambda_1$  to the minor pathway and  $\lambda_2$  to the major pathway, the model would predict a steeper equilibrium unfolding transition between  $U_{eq}$  and  $I_{eq}$ , inconsistent with the observed equilibrium measurements. Since WT\* SNase exhibits kinetic behavior on this time-scale very similar to Trp76 SNase (see Figure 6), we applied the same

scheme to the WT\* SNase. The microscopic rate constants thus determined are listed in Table 5. We found that a more complicated scheme including a second intermediate along the minor pathway gives slightly better fits, but we chose to present the simpler Scheme 4, which appears to be the simplest possible scheme that fully accounts for the kinetic and thermodynamic data (see Discussion).

We also considered the possibility that phases 1 and 2 are due to sequential intermediates located on the major pathway while phase 5 represents the interconversion between  $U'$  and  $M$  states. However, in this case the total  $m$ -value for the formation of  $I_2$  from  $U$ , estimated from the  $m$ -values for the intervening steps ( $m_{UI}^\ddagger + m_{IU}^\ddagger + m_{U'I'}^\ddagger + m_{I'U'}^\ddagger$ ), would be at least  $2.2 \text{ kcal mol}^{-1} \text{ M}^{-1}$ , which is much larger than the  $m_{UI}$ -value of  $0.96 \text{ kcal mol}^{-1} \text{ M}^{-1}$  measured at equilibrium (Table 5). Thus,  $\lambda_1$  and  $\lambda_2$  cannot be attributed to sequential steps.

The remaining four phases were modeled as described by Walkenhorst *et al.*<sup>25</sup> First, we consider the major folding pathway. In the refolding reaction, the curvature of  $\lambda_4$  at low urea concentrations is consistent with accumulation of at least one intermediate ( $I_2$ ) ( $\lambda_4 \sim k_{I1I2}/(k_{I1I2} + k_{I2I1}) \times k_{I2M}$ ). Similarly, the curvature in the unfolding limb of Trp76 SNase requires at least one intermediate ( $M$ ) to bring about the switch of the rate-limiting step of the unfolding reaction ( $\lambda_u \sim k_{MI2}/(k_{MI2} + k_{MN}) \times k_{NM}$ ). The previous study clearly showed curvature in the GuHCl-induced unfolding rate of H124L and a proline-free SNase.<sup>25</sup> We assume the same phenomenon occurs for WT\* SNase, but the curvature in the unfolding profile is less pronounced because of the weaker denaturing strength of urea compared to GuHCl. In contrast to the major folding pathway, the kinetic behavior of the minor pathway is well accounted for without adding other intermediates. Thus, phase 5 is attributed to the interconversion between  $I'$  and  $M$ .

**Table 5.** Kinetic parameters estimated by modeling the folding kinetics of WT\* and Trp76 SNase, based on Scheme 4

Reaction $i \rightarrow j$	WT* SNase		Trp76 SNase	
	Rates ( $k_{ij}^0$ ) ( $s^{-1}$ ) <sup>a</sup>	$m_{ij}^\ddagger$ -value ( $\text{kcal mol}^{-1} \text{ M}^{-1}$ ) <sup>b</sup>	Rates ( $k_{ij}^0$ ) ( $s^{-1}$ ) <sup>a</sup>	$m_{ij}^\ddagger$ -value ( $\text{kcal mol}^{-1} \text{ M}^{-1}$ ) <sup>b</sup>
$U \rightarrow I_1$	18,000	-0.56	18,000	-0.56
$I_1 \rightarrow U$	500	0.4	500	0.4
$I_1 \rightarrow I_2$	30	0	40	0
$I_2 \rightarrow I_1$	25	0.65	15	1.15
$I_2 \rightarrow M$	22	-0.45	15	-0.3
$M \rightarrow I_2^c$	7.5	0.4	90	0.8
$M \rightarrow N^c$	50,000	0	50,000	0
$N \rightarrow M$	1.8	0.04	20	0.08
$U' \rightarrow I'$	6500	-1.1	6500	-1.1
$I' \rightarrow U'$	15	0.5	100	0.2
$I' \rightarrow M$	1	-0.32	2	-1.2
$M \rightarrow I'$	1	0.2	0.1	0.2
$U \rightarrow U'$	0.00004	0	0.00004	0
$U' \rightarrow U$	0.001	0	0.001	0

<sup>a</sup> Rate constant for a given process in the absence of urea.

<sup>b</sup> Kinetic  $m$ -values according to equation (1).

<sup>c</sup> Only the ratio  $k_{MN}/k_{MI}$  is uniquely determined.

As an additional test of the model, we calculated the time-course of folding on the basis of the microscopic rate constants (Table 5), which were optimized by fitting the observable rates (Figure 7). As indicated by the broken lines in Figure 6, the model provides an adequate simultaneous fit of the whole family of kinetic traces at different denaturant concentrations, both in the case of WT\* and Trp76 SNase. In addition, the optimized kinetic parameters quantitatively reproduce the population of the equilibrium states,  $N$ ,  $I_{eq}$  and  $U_{eq}$  (broken lines in Figure 3c and d), which demonstrates an excellent agreement between kinetic and equilibrium thermodynamic parameters. Because some of the states assigned in the kinetic measurements cannot be resolved under equilibrium conditions, we combined  $U$  and  $U'$  in  $U_{eq}$ , and  $I_1$ ,  $I_2$  and  $I'$  in  $I_{eq}$ . The contribution of  $M$  to the equilibrium population is negligible because it is always a high-energy state with negligible population. Table 2 shows excellent agreement between the equilibrium thermodynamic parameters predicted by the kinetic modeling and those obtained by fitting the equilibrium unfolding transitions. Accumulation of an equilibrium intermediate for Trp76 SNase can be attributed to the shift of the minimum in  $\lambda_4$  to lower denaturant concentration compared to the minima in  $\lambda_1$  and  $\lambda_2$ , giving rise to an increase in the stability of the kinetic intermediates relative to  $N$ . On the other hand, in the case of WT\* SNase, the minima for  $\lambda_1$  and  $\lambda_2$  occur below that of  $\lambda_4$ , giving rise to a highly cooperative equilibrium unfolding with negligible accumulation of intermediates.

## Discussion

### Early stages of the folding of WT\* and Trp76 SNase

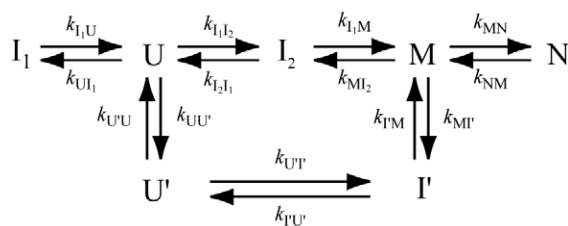
Evidence for accumulation of intermediates at early stages of SNase folding has been reported previously, based on the observation of kinetically unresolved changes (burst phase) in CD<sup>24</sup> and fluorescence labeling experiments,<sup>46</sup> and by the observation of significant protection from solvent exchange within 10 ms of refolding in NMR-detected pulsed hydrogen exchange experiments.<sup>22,23</sup> Previous stopped-flow folding experiments on SNase variants containing the wild-type Trp140 showed only minor discrepancies between the fluorescence intensity extrapolated to a folding time  $t = 0$  and that of the initial unfolded state at pH 2.0 (10–15% of total change, which is largely accounted for by the intrinsic pH dependence of Trp fluorescence).<sup>25,31</sup> These studies showed that Trp140 is a poor reporter for monitoring the structural events before the rate-limiting step of SNase folding. Thus, we constructed a variant containing a single Trp at position 76 (F76W/W140H), a buried position at the edge of the hydrophobic core enclosed by the N-terminal

$\beta$ -barrel, which proved to be a more sensitive probe for observing early folding events.

The fluorescence of Trp76 SNase shows a significant increase within 100  $\mu$ s of refolding, indicating accumulation of an intermediate in which Trp76 is partially buried. By monitoring the fluorescence changes associated with ANS binding, we were able to greatly amplify the signal changes during these initial stages of folding, confirming the formation of an intermediate with solvent-exposed hydrophobic surface area or a loosely packed hydrophobic core. Previous studies showed that ANS may perturb the folding reaction, and meaningful results on the late stages of folding can usually be obtained only by using a pulse labeling technique.<sup>43</sup> However, ANS turned out to be an excellent probe for monitoring early folding events in SNase, based on our observation that the apparent rate constants in the presence of ANS reflect the rates of folding measured *via* intrinsic tryptophan fluorescence, provided that the ANS concentration is high enough for its association rate to exceed the folding rate.

Systematic folding/unfolding experiments of WT\* and Trp76 SNase showed that the folding kinetics at low urea concentrations consists of five phases (excluding the slowest phase, which has been assigned to a minor population of molecules occurring from the folding rate-limited by isomerization of prolyl-peptide bonds<sup>25,31</sup>). Despite its complexity, Scheme 4 is a minimal extension of the previously proposed Scheme 3,<sup>25</sup> which is necessary to account for the new sub-millisecond process (phase 1) detected by both intrinsic Trp and ANS fluorescence. Scheme 4 accounts for all experimental data for both WT\* and Trp76 SNase, including the rates of the five main phases (Figure 7) as well as the family of kinetic traces in the presence of ANS (Figure 6; broken lines).

At urea concentrations near 1.5 M, phases 1 and 2 show a subtle curvature for both proteins (Figure 7). We were able to account for this effect by placing an additional intermediate between  $U$  ( $U'$ ) and  $I_1$  ( $I'$ ) on each folding pathway. This resulted in slightly improved quality of fitting, especially for the series of kinetic traces monitored by ANS fluorescence. However, the properties of these hypothetical earliest intermediates are very similar to those of  $U$  in terms of ANS binding and Trp fluorescence, and the corresponding time constant of the formation is  $< 50 \mu$ s. Since introduction of the additional states has only a minor effect, we



Scheme 5.

chose the simpler model (Scheme 4) for further discussion.

In order to test whether  $I_1$  is an ensemble of on-pathway or off-pathway intermediates, we examined an off-pathway version of Scheme 4 (Scheme 5). As expected from the rather weak coupling between phases 1 and 3, the behavior predicted by Scheme 5 is essentially indistinguishable from that of Scheme 4. This is because the interconversion between U and  $I_1$  is much more rapid than that between U (or  $I_1$  in Scheme 4) and  $I_2$ , so that a pre-equilibrium is rapidly established between U and  $I_1$ , as observed in other studies.<sup>15,47</sup>

### The properties of the equilibrium intermediate and its relationship to kinetic intermediates

The equilibrium unfolding of Trp76 SNase revealed accumulation of an intermediate under moderately denaturing conditions ( $\sim 2$  M urea). A number of studies described equilibrium intermediates in the denaturant and temperature-induced unfolding transition of SNase variants.<sup>37–40</sup> These results are explained by a model involving an equilibrium intermediate consisting of the partially structured  $\beta$ -barrel domain uncoupled from the  $\alpha$ -helical domain. This model is based on equilibrium fluorescence data indicating that certain variants of full-length SNase (especially V66W) show deviation from two-state behavior, but can be modeled by a three-state mechanism. Moreover, the 1–136 fragment shows a single sigmoidal transition corresponding to the second transition of the full-length protein (at higher denaturant concentration). Since 1–136 fragments of SNase contain considerable  $\beta$ -structure uncoupled from the  $\alpha$ -helical domain in the absence of denaturant,<sup>48,49</sup> their unfolding transition reflects disruption of the  $\beta$ -barrel domain. This model can also explain the multi-state unfolding behavior of Trp76 SNase.

Trp76 is located in the loop between strands IV and V. The contact between the  $\beta$ -barrel and  $\alpha$ -helical domains is known to be stabilized by two residues in this loop, Glu75 and Asp77, which form ionic interaction with His121<sup>50</sup> and hydrogen bonds to Thr120,<sup>51</sup> respectively. A previous study showed that disruption of these interactions by E75A or D77A substitutions resulted in accumulation of experimentally detectable equilibrium intermediates.<sup>38</sup> It is likely that the replacement of Phe76 with the bulkier Trp weakens these specific interactions to some extent, causing a selective destabilization of the native state in Trp76 SNase relative to WT\* SNase. In addition, the W140H substitution also contributes to the destabilization of the native state of Trp76 SNase. Since Trp140 in WT\* SNase is largely buried and involved in extensive contacts with both polar and hydrophobic residues at the C-terminal end of helix H3 (Figure 1), the Trp to His substitution may affect the stability of the  $\alpha$ -helical domain to a larger extent than that of the  $\beta$ -barrel domain. The thermal unfolding experiments showed that W140H

substitution destabilizes the native state by 0.4 kcal mol<sup>-1</sup> while the subsequent F76W substitution results in a further 0.6 kcal mol<sup>-1</sup> decrease in stability (Table 1). From the viewpoint of fluorescence properties, the slightly more intense fluorescence of  $I_{eq}$  accompanied by a  $\sim 6$  nm blue shift in comparison with  $U_{eq}$  suggests a partially solvent-shielded environment of the Trp76 side-chain arising from residual structure in the N-terminal domain of  $I_{eq}$ . Moreover, the free energy,  $\Delta G_{UI} = 2.08$  kcal mol<sup>-1</sup>, for the  $U_{eq} \leftrightarrow I_{eq}$  transition of Trp76 SNase is in close agreement with that of SNase V66W ( $\Delta G_{UI} = 2.21$  kcal mol<sup>-1</sup>).<sup>40</sup>

On the other hand, the urea-induced unfolding equilibrium of WT\* SNase is well approximated by a two-state model while the kinetic model predicts at most 5% population of  $I_{eq}$  (Figure 3c). The  $m$ -value of the  $U_{eq} \leftrightarrow N$  transition,  $m_{UN}$ , of Trp76 SNase is 1.4-fold larger than that of WT\* SNase. The difference in  $m_{UN}$  between WT\* and Trp76 SNase apparently arises from the difference in  $m_{I_{eq}N}$  (Table 2), and especially in  $m_{I_{2I}^\ddagger}$  and  $m_{MI_2^\ddagger}$  (Table 5), based on the kinetic model of WT\* SNase. However,  $m_{MI_2^\ddagger}$  is not uniquely defined due to lack of constraints for this kinetic parameter (we can only define the ratio  $k_{MI_2}/k_{MN}$ ), so that  $m_{MI_2^\ddagger}$  is likely to have a large error, which may partly account for the apparent difference. Trp140 in the  $\alpha$ -helical domain of WT\* SNase is expected to be less sensitive to the structure changes in the  $\beta$ -barrel domain occurring during the  $U \leftrightarrow I_{eq}$  transition than those occurring during the  $I_{eq} \leftrightarrow N$  transition, where the  $\alpha$ -helical domain is uncoupled from the rest of molecule. Thus, the unfolding transition probed by Trp140 corresponds mainly to the first transition of Trp76 SNase unfolding, as pointed out previously.<sup>37</sup> Another possibility of the difference in  $m_{UN}$  is the stability difference of helix H3 between WT\* and Trp76 SNase. The destabilization by W140H substitution in Trp76 SNase may result in partial unfolding or fraying of helix H3 in the intermediate state, giving rise to an increase in the accessible surface area of Trp76 SNase between the native and the intermediate states in comparison with WT\* SNase. This accounts for the difference in  $m_{UN}$  (especially  $m_{I_{eq}N}$ ), since  $m$ -values are well correlated with the change in accessible surface area associated with unfolding transitions.

The equilibrium intermediate,  $I_{eq}$ , corresponds to an ensemble of kinetic intermediates consisting of  $I_1$ ,  $I_2$  and  $I'$ , with  $I_1$  making the dominant contribution (92% of total population of  $I_{eq}$  at 1.96 M). This assignment is consistent with the difference in urea concentrations where  $\lambda_1$  and  $\lambda_4$  go through a minimum in Trp76 SNase folding/unfolding (Figure 7); around 2 M urea, folding from U as well as unfolding from M is preferred so that intermediate states are preferentially populated in comparison with N or U. In fact,  $\Delta G_{UI} (= -0.13$  kcal mol<sup>-1</sup>),  $\Delta G_{UN} (= -0.52$  kcal mol<sup>-1</sup>) at 2 M urea are small as well as close to each

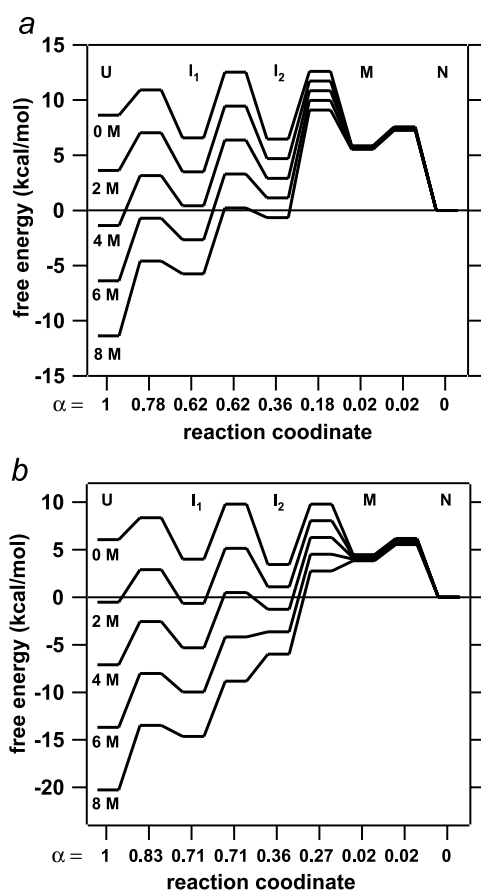


**Figure 8.** Free energy diagrams of WT\* (a) and Trp76 SNase (b) showing the effects of urea on the energy levels and transition states predicted by quantitative analysis of the folding and unfolding kinetics. The  $\alpha$  values indicate the change in solvent-accessible surface area relative to N.

other, that is N,  $I_1$  and U have similar free energies at 2 M urea (Figure 8). In other words, selective destabilization of N relative to U results in significant accumulation of equilibrium intermediates in Trp76 SNase at certain urea concentrations. On the other hand, the native state of WT\* SNase is more stable than  $I_{eq}$ , resulting in negligible population of equilibrium intermediates. Quantitative modeling of the folding kinetics of WT\* and Trp76 SNase showed that the kinetic parameters fully reproduce the equilibrium properties (Figure 3c and d), which establishes the connection between kinetic and equilibrium intermediates.

This work, together with a previous study,<sup>25</sup> identified three intermediates ( $I_1$ ,  $I_2$  and M) on the major folding pathway while one intermediate ( $I'$ ) is encountered on a minor parallel folding pathway.  $I_1$  accumulates within 100  $\mu$ s of refolding and contains a partially consolidated core (probably within the  $\beta$ -barrel domain) able to bind ANS.  $I_2$ , which was previously shown to contain a stable hydrogen-bonded  $\beta$ -hairpin comprising strands II and III, is populated over the 10 ms time-range.<sup>23,25</sup> M is a native-like state giving rise to a bend (rollover) in the unfolding kinetics.<sup>25</sup> Finally,

$I'$  is a compact state (based on its ability to bind ANS) belonging to a minor population of molecules folding along a parallel pathway.  $I'$  appears within about 250  $\mu$ s of refolding and decays on the 1 s time scale. The origin of this minor species is not clear at this time. Since a proline-free variant of SNase also shows evidence for a parallel folding pathway, Walkenhorst *et al.*<sup>25</sup> tentatively assigned it to a population of molecules containing non-proline *cis* peptide bonds. However, other sources of heterogeneity, such as alternative chain topologies or side-chain packing arrangements cannot be ruled out as long as they give rise to slowly interconverting populations ( $\sim$ 100 ms or longer).

### Broader implications

One of the motivations for focusing on the early stages of folding is to address the critical question whether the initial conformational events reflect a specific barrier-limited folding step or a non-specific collapse of the polypeptide chain. All the results obtained here are characterized by multi-exponential kinetics, and quantitative kinetic modeling shows that the data are fully consistent with a mechanism involving several partially structured states separated by kinetic barriers, as demonstrated for other proteins.<sup>12–15,17</sup>

The earliest folding phase detected here is especially prominent in the ANS-detected kinetics of both WT\* and Trp76 SNase, but is more difficult to detect by intrinsic fluorescence (Figure 5). Thus, as in the case of ACBP,<sup>15</sup> detection of some early folding events relies not only on sufficient temporal resolution, but also the availability of suitable conformational probes. Fluorescence energy transfer and ANS binding are sensitive to changes in overall chain dimensions and hydrophobic core formation, respectively, and are thus especially useful for characterizing early stages of folding.

With a time constant  $\tau = 75 \mu$ s, the initial folding phase of SNase occurs on the same time-scale as that of cytochrome *c* ( $\tau = 50–90 \mu$ s)<sup>12,17</sup> and ACBP ( $\tau = 80 \mu$ s),<sup>15</sup> but is somewhat faster than the early folding phases reported for Im7 ( $\tau = 150 \mu$ s<sup>14</sup>) and protein G ( $\tau = 600 \mu$ s<sup>13</sup>). Considering the fact that these proteins cover a variety of structural types, including predominantly  $\alpha$ -helical (ACBP, cytochrome *c* and Im7) and mixed  $\alpha$ - $\beta$  proteins (protein G and SNase), there appears to be no simple relationship between the time-scale of early folding events and secondary structure content. There is also no apparent correlation between the initial folding times and protein size, as one might have expected if the early phase involved a non-specific polymer collapse. This is dramatically illustrated by comparing SNase (149 residues;  $\tau = 75 \mu$ s) with protein G (57 residues;  $\tau = 600 \mu$ s), indicating that specific structural and topological features have profound effect already during early stages of folding. One possible scenario is that the 75  $\mu$ s phase of SNase detected by Trp76 and ANS fluorescence

reflects a relatively local structural event involving parts of the  $\beta$ -barrel, which is composed of anti-parallel strands while the fluorescence of Trp43 in protein G may report on a more global conformational change involving the parallel pairing of C-terminal  $\beta$ -strands. While we do not expect any correlation between contact order (a metric of topological complexity) and the rate-limiting folding step for proteins with multi-state folding kinetics,<sup>52</sup> this concept would be applicable to fast folding steps if native-like chain topology is formed during these early stages. This conclusion is supported by the observation that some small proteins (or isolated domains of larger proteins) can complete the process of folding on a time-scale comparable to the early stages of folding for some of the multi-state proteins mentioned above.<sup>53–56</sup>

## Materials and Methods

### Chemicals

Urea was ultra-pure grade from ICN. All other chemicals were reagent grade. Urea concentration was determined by refractive index measurement<sup>57</sup> using a Reichert-Jung Mark II Abbe refractometer (Leica, Inc., New York).

### Mutagenesis and protein purification

Expression plasmids containing WT\* SNase, four Trp-free variants (W140H, W140F, W140Y and W140L) and Trp76 SNase (F76W/W140H), all in the P47G/P117G/H124L background, were prepared by using a Quik-Change Site-Directed mutagenesis kit (Stratagene, CA). WT\* and Trp76 SNase were prepared and purified as described,<sup>58</sup> except that the cells were grown on LB medium, and that BioRex 70 (Bio-Rad, CA) was used as cation-exchange resin instead of C25 CM-Sephadex.

### Thermal unfolding measurements

The thermal unfolding transitions of WT\* SNase, four Trp-free SNase variants (W140H, W140F, W140Y and W140L) and Trp76 SNase were measured by monitoring the change in far-UV CD at 222 nm on increasing the temperature from 15 °C to 80 °C. The data were recorded in 2 mm quartz cuvettes on an AVIV 62DS spectropolarimeter equipped with a thermoelectric sample-holder. The solutions contained  $\sim 10 \mu\text{M}$  protein, 25 mM sodium phosphate (pH 7.0), 50 mM NaCl, 0.5 mM EDTA. Free energies at 20 °C were calculated based on the Gibbs–Helmholtz equation using a constant value of  $\Delta C_p = 1.67 \text{ kcal mol}^{-1} \text{ K}^{-1}$ .

### Equilibrium measurements of CD spectra

The CD spectra of WT\* and Trp76 SNase were collected over a range from 190 nm to 250 nm (far-UV region) and from 250 nm to 310 nm (near-UV region) at pH 7.0 as well as 2.0 and 15 °C. The data were recorded every 1 nm using 2 mm quartz cuvettes. The protein concentrations were 2–10  $\mu\text{M}$  and 50–75  $\mu\text{M}$  for the measurements in the far and near-UV regions, respectively. The

solution contained 20 sodium phosphate (pH 7.0) or 10 mM HCl/phosphoric acid (pH 2.0).

### Equilibrium unfolding measurements monitored by intrinsic tryptophan fluorescence

WT\* or Trp76 SNase solutions containing various concentrations of urea ranging from 0 M to 7.5 M in steps of 0.2–0.4 M were prepared in a flow-cell by mixing a 5  $\mu\text{M}$  protein solution in  $\sim 100$  mM sodium acetate (pH 5.2) with an identical solution containing 8 M urea, using an OLIS (Jefferson, GA) automatic titration device. At every urea concentration prepared, the fluorescence emission spectrum from 300 nm to 450 nm was recorded on a PTI (South Brunswick, NJ) QM-2000 spectrofluorometer, using an excitation wavelength of 288 nm. Samples were incubated for 5–15 minutes before each measurement at 15 °C. The global fitting of fluorescence-detected unfolding transition curves *versus* wavelength was carried out by using the global fitting procedure of the IGOR software package (WaveMetrics, Inc., Lake Oswego, OR).

### Kinetic measurements

For refolding experiments, stock solutions of acid-unfolded WT\* or Trp76 SNase were prepared in 20 mM phosphoric acid (pH 2.0). The refolding reaction was initiated by tenfold dilution of the acid-unfolded protein with refolding buffer containing 100 mM sodium acetate with appropriate concentrations of urea and ANS (pH 5.3), giving a final pH of 5.2 after mixing. For salt-induced refolding, the acid-unfolded protein stock solution was diluted tenfold with a solution containing 20 mM phosphoric acid, 1.1 M KCl with various concentrations of ANS (pH 2.0). For the ANS binding reaction to the A-state, the protein stock solution was diluted tenfold with solutions containing appropriate concentrations of ANS, 20 mM phosphoric acid and 1.0 M KCl (pH 2.0). The protein stock solution for unfolding experiments contained 100 mM sodium acetate (pH 5.2). Unfolding reactions were initiated by diluting the stock solution with the same buffer containing the appropriate concentration of urea (pH 5.2). For the refolding and unfolding reactions measured by Trp fluorescence (in the absence of ANS), the time-dependent fluorescence change was monitored with a 324 nm high-pass filter, exciting Trp fluorescence at 288 nm using a monochromator with a 4 nm band pass. In experiments involving ANS, the time-dependent ANS fluorescence change was monitored with a 418 nm high-pass filter upon excitation at 366 nm. All the experiments were conducted at 15 °C. Continuous-flow measurements were carried out as described by Shastry *et al.*<sup>11</sup> with a flow rate of 1.04 ml/s. Stopped-flow measurements were carried out on a BioLogic (Grenoble, France) SFM-4 instrument. The dead times of continuous-flow and stopped-flow devices were 100  $\mu\text{s}$  and 2.4 ms, respectively, calibrated by measuring the quenching of NATA fluorescence by *N*-bromosuccinimide at several quencher concentrations.<sup>11,59</sup>

### Kinetic modeling

Standard numeric methods were used to solve the system of linear differential equations describing a particular kinetic scheme, using IGOR software to determine the eigenvalues and eigenvectors of the

corresponding rate matrix.<sup>60</sup> The kinetic parameters were manually optimized to fit the experimental data. The ANS concentration dependence of the apparent rate constants of ANS binding to the A-state of Trp76 SNase and the pH-induced refolding reaction under native or A-state conditions were modeled using Schemes 1 and 2 for binding and refolding reactions, respectively. For the binding reaction, pseudo-first-order conditions were assumed where the association rate constant ( $k_{\text{on}}$ ) is linearly dependent on ANS concentration while the dissociation rate constant ( $k_{\text{off}}$ ) is ANS concentration-independent. The microscopic rate constants ( $k_{\text{U}^{\text{acc}}}$  and  $k_{\text{U}^{\text{accU}}}$ ) on the refolding reaction were assumed to be ANS concentration-independent.

Several kinetic schemes were tested for modeling the measured kinetic and equilibrium data for WT\* and Trp76 SNase folding. The urea concentration dependence of the microscopic rate constants were assumed to follow equation (1):

$$\ln(k_{ij}) = \ln(k_{ij}^0) + (m_{ij}^\ddagger/RT)[\text{urea}] \quad (1)$$

where  $k_{ij}^0$  is the microscopic rate constant in the absence of urea and  $m_{ij}^\ddagger$  is the corresponding slope.<sup>61</sup> The various sets of the microscopic rate constants and the slope were explored systematically to model the apparent rates and amplitudes observed in the kinetic measurements, as well as the equilibrium thermodynamic parameters measured in the equilibrium unfolding experiments, based on the associated rate matrix. Free energy diagrams were calculated from the elementary rate parameters obtained. The activation energy for crossing the barriers between states was calculated as follows:

$$\Delta G_{ij}^\ddagger = -RT \ln(k_{ij}^0/A_0) - m_{ij}^\ddagger[\text{urea}] \quad (2)$$

using an arbitrary value of  $1 \times 10^6 \text{ M}^{-1} \text{ s}^{-1}$  for the pre-exponential factor,  $A_0$ .

## Acknowledgements

We thank Drs Z. Bu and D. Samuel for their careful reading of the manuscript. The work was supported by NIH grant GM56250 to H.R., and NIH core grant CA06927 and an appropriation from the Commonwealth of Pennsylvania to the Fox Chase Cancer Center. The Spectroscopy Support Facility provided access to fluorescence and CD spectrometers.

## References

- Roder, H. & Colón, W. (1997). Kinetic role of early intermediates in protein folding. *Curr. Opin. Struct. Biol.* **7**, 15–28.
- Jackson, S. E. (1998). How do small single-domain proteins fold? *Fold. Des.* **3**, R81–R91.
- Khorasanizadeh, S., Peters, I. D. & Roder, H. (1996). Evidence for a three-state model of protein folding from kinetic analysis of ubiquitin variants with altered core residues. *Nature Struct. Biol.* **3**, 193–205.
- Baldwin, R. L. (1996). On-pathway versus off-pathway folding intermediates. *Fold. Des.* **1**, R1–R8.
- Baldwin, R. L. & Rose, G. D. (1999). Is protein folding hierarchic? II. Folding intermediates and transition states. *Trends Biochem. Sci.* **24**, 77–83.
- Sosnick, T. R., Shtilerman, M. D., Mayne, L. & Englander, S. W. (1997). Ultrafast signals in protein folding and the polypeptide contracted state. *Proc. Natl Acad. Sci. USA*, **94**, 8545–8550.
- Krantz, B. A., Mayne, L., Rumbley, J., Englander, S. W. & Sosnick, T. R. (2002). Fast and slow intermediate accumulation and the initial barrier mechanism in protein folding. *J. Mol. Biol.* **324**, 359–371.
- Regenfuss, P., Clegg, R. M., Fulwyler, M. J., Barrantes, F. J. & Jovin, T. M. (1985). Mixing liquids in microseconds. *Rev. Sci. Instrum.* **56**, 283–290.
- Takahashi, S., Yeh, S.-R., Das, T. K., Chan, C.-K., Gottfried, D. S. & Rousseau, D. L. (1997). Folding of cytochrome c initiated by submillisecond mixing. *Nature Struct. Biol.* **4**, 44–50.
- Chan, C.-K., Hu, Y., Takahashi, S., Rousseau, D. L., Eaton, W. A. & Hofrichter, J. (1997). Submillisecond protein folding kinetics studied by ultrarapid mixing. *Proc. Natl Acad. Sci. USA*, **94**, 1779–1784.
- Shastry, M. C. R., Luck, S. D. & Roder, H. (1998). A continuous-flow capillary mixer to monitor reactions on the microsecond time scale. *Biophys. J.* **74**, 2714–2721.
- Shastry, M. C. R. & Roder, H. (1998). Evidence for barrier-limited protein folding kinetics on the microsecond time scale. *Nature Struct. Biol.* **5**, 385–392.
- Park, S.-H., Shastry, M. C. R. & Roder, H. (1999). Folding dynamics of the B1 domain of protein G explored by ultrarapid mixing. *Nature Struct. Biol.* **6**, 943–947.
- Capaldi, A. P., Shastry, R. M. C., Kleantous, C., Roder, H. & Radford, S. E. (2001). Ultra-rapid mixing experiments reveal that Im7 folds via an on-pathway intermediate. *Nature Struct. Biol.* **8**, 68–72.
- Teilum, K., Maki, K., Kragelund, B. B., Poulsen, F. M. & Roder, H. (2002). Early kinetic intermediate in the folding of acyl-CoA binding protein detected by fluorescence labeling and ultrarapid mixing. *Proc. Natl Acad. Sci. USA*, **99**, 9807–9812.
- Shastry, M. C. R., Sauder, J. M. & Roder, H. (1998). Kinetic and structural analysis of submillisecond folding events in cytochrome c. *Accs Chem. Res.* **31**, 717–725.
- Hagen, S. J. & Eaton, W. A. (2000). Two-state expansion and collapse of a polypeptide. *J. Mol. Biol.* **297**, 781–789.
- Akiyama, S., Takahashi, S., Ishimori, K. & Morishima, I. (2000). Stepwise formation of alpha-helices during cytochrome c folding. *Nature Struct. Biol.* **7**, 514–520.
- Kuwata, K., Shastry, R., Cheng, H., Hoshino, M., Batt, C. A., Goto, Y. & Roder, H. (2001). Structural and kinetic characterization of early folding events in beta-lactoglobulin. *Nature Struct. Biol.* **8**, 151–155.
- Pollack, L., Tate, M. W., Darnton, N. C., Knight, J. B., Gruner, S. M., Eaton, W. A. & Austin, R. H. (1999). Compactness of the denatured state of a fast-folding protein measured by submillisecond small-angle X-ray scattering. *Proc. Natl Acad. Sci. USA*, **96**, 10115–10117.
- Akiyama, S., Takahashi, S., Kimura, T., Ishimori, K., Morishima, I., Nishikawa, Y. & Fujisawa, T. (2002). Conformational landscape of cytochrome c folding studied by microsecond-resolved small-angle X-ray scattering. *Proc. Natl Acad. Sci. USA*, **99**, 1329–1334.
- Jacobs, M. D. & Fox, R. O. (1994). Staphylococcal nuclease folding intermediate characterized by

- hydrogen exchange and NMR spectroscopy. *Proc. Natl Acad. Sci. USA*, **91**, 449–453.
23. Walkenhorst, W. F., Edwards, J. A., Markley, J. L. & Roder, H. (2002). Early formation of a beta hairpin during folding of staphylococcal nuclease H124L as detected by pulsed hydrogen exchange. *Protein Sci.* **11**, 82–91.
  24. Sugawara, T., Kuwajima, K. & Sugai, S. (1991). Folding of staphylococcal nuclease A studied by equilibrium and kinetic circular dichroism spectra. *Biochemistry*, **30**, 2698–2706.
  25. Walkenhorst, W. F., Green, S. M. & Roder, H. (1997). Kinetic evidence for folding and unfolding intermediates in staphylococcal nuclease. *Biochemistry*, **63**, 5795–5805.
  26. Hynes, T. R. & Fox, R. O. (1991). The crystal structure of staphylococcal nuclease refined at 1.7 Å resolution. *Proteins: Struct. Funct. Genet.* **10**, 92–105.
  27. Schechter, A. N., Chen, R. F. & Anfinsen, C. B. (1970). Kinetics of folding of staphylococcal nuclease. *Science*, **167**, 886–887.
  28. Chen, H. M., You, J. L., Markin, V. S. & Tsong, T. Y. (1991). Kinetic analysis of the acid and the alkaline unfolded states of staphylococcal nuclease. *J. Mol. Biol.* **220**, 771–778.
  29. Kuwajima, K., Okayama, N., Yamamoto, K., Ishihara, T. & Sugai, S. (1991). The Pro117 to glycine mutation of staphylococcal nuclease simplifies the unfolding–folding kinetics. *FEBS Letters*, **290**, 135–138.
  30. Nakano, T., Antonino, L. C., Fox, R. O. & Fink, A. L. (1993). Effect of proline mutations on the stability and kinetics of folding of staphylococcal nuclease. *Biochemistry*, **32**, 2534–2541.
  31. Maki, K., Ikura, T., Hayano, T., Takahashi, N. & Kuwajima, K. (1999). Effects of proline mutations on the folding of staphylococcal nuclease. *Biochemistry*, **38**, 2213–2223.
  32. Evans, P. A., Dobson, C. M., Kautz, R. A., Hatfull, G. & Fox, R. O. (1987). Proline isomerism in staphylococcal nuclease characterized by nmr and site-directed mutagenesis. *Nature*, **329**, 266–268.
  33. Hinck, A. P., Eberhardt, E. S. & Markley, J. L. (1993). NMR strategy for determining Xaa-Pro-peptide bond configurations in proteins: mutants of staphylococcal nuclease with altered configuration at proline-117. *Biochemistry*, **32**, 11810–11818.
  34. Alexandrescu, A. T., Ulrich, E. L. & Markley, J. L. (1989). Hydrogen-1 NMR evidence for three interconverting forms of staphylococcal nuclease: effects of mutations and solution conditions on their distribution [erratum: *Biochemistry* (1989) 28:3628]. *Biochemistry*, **28**, 204–211.
  35. Shortle, D. (1995). Staphylococcal nuclease: a showcase of *m*-value effects. *Advan. Protein Chem.* **46**, 217–247.
  36. Shortle, D. (2002). The expanded denatured state: an ensemble of conformations trapped in a locally encoded topological space. *Advan. Protein Chem.* **62**, 1–23.
  37. Gittis, A. G., Stites, W. E. & Lattman, E. E. (1993). The phase transition between a compact denatured state and a random coil state in Staphylococcal nuclease is first-order. *J. Mol. Biol.* **232**, 718–724.
  38. Carra, J. H., Anderson, E. A. & Privalov, P. L. (1994). Three-state thermodynamic analysis of the denaturation of staphylococcal nuclease mutants. *Biochemistry*, **33**, 10842–10850.
  39. Eftink, M. R., Ionescu, R., Ramsey, G. D., Wong, C.-Y., Wu, J. Q. & Maki, A. H. (1996). Thermodynamics of the unfolding and spectroscopic properties of the V66W mutant of *Staphylococcal* nuclease and its 1-136 fragment. *Biochemistry*, **35**, 8084–8094.
  40. Ionescu, R. M. & Eftink, M. R. (1997). Global analysis of the acid-induced and urea-induced unfolding of staphylococcal nuclease and two of its variants. *Biochemistry*, **36**, 1129–1140.
  41. Semisotnov, G. V., Rodionova, N. A., Kutysenko, V. P., Ebert, B., Blanck, J. & Ptitsyn, O. B. (1987). Sequential mechanism of refolding of carbonic anhydrase B. *FEBS Letters*, **224**, 9.
  42. Shi, L., Palleros, D. R. & Fink, A. L. (1994). Protein conformational changes induced by 1,1'-bis(4-anilino-5-naphthalenesulfonic acid): preferential binding to the molten globule of DnaK. *Biochemistry*, **33**, 7536–7546.
  43. Engelhard, M. & Evans, P. A. (1995). Kinetics of interaction of partially folded proteins with a hydrophobic dye: evidence that molten globule character is maximal in early folding intermediates. *Protein Sci.* **4**, 1553–1562.
  44. Hinck, A. P., Walkenhorst, W. F., Truckses, D. M. & Markley, J. L. (1996). NMR and mutagenesis investigations of a model *cis:trans* peptide isomerization reaction: Xaa<sup>116</sup>-Pro<sup>117</sup> of staphylococcal nuclease and its role in protein stability and folding. In *Biological NMR Spectroscopy* (Markley, J. L. & Opella, S. J., eds), pp. 133–160, Oxford University Press, Oxford.
  45. Shortle, D. (1986). Guanidine hydrochloride denaturation studies of mutant forms of staphylococcal nuclease. *J. Cell. Biochem.* **30**, 281–289.
  46. Nishimura, C., Riley, R., Eastman, P. & Fink, A. L. (2000). Fluorescence energy transfer indicates similar transient and equilibrium intermediates in staphylococcal nuclease folding. *J. Mol. Biol.* **299**, 1133–1146.
  47. Mizuguchi, M., Arai, M., Ke, Y., Nitta, K. & Kuwajima, K. (1998). Equilibrium and kinetics of the folding of equine lysozyme studied by circular dichroism spectroscopy. *J. Mol. Biol.* **283**, 265–277.
  48. Shortle, D. & Abeygunawardana, C. (1993). NMR analysis of the residual structure in the denatured state of an unusual mutant of staphylococcal nuclease. *Structure*, **1**, 121–134.
  49. Alexandrescu, A. T., Gittis, A. G., Abeygunawardana, C. & Shortle, D. (1995). NMR structure of a stable “OB-fold” sub-domain isolated from staphylococcal nuclease. *J. Mol. Biol.* **250**, 134–143.
  50. Loll, P. J. & Lattman, E. E. (1989). The crystal structure of the ternary complex of staphylococcal nuclease, Ca<sup>2+</sup>, and the inhibitor pdTp, refined at 1.65 Å. *Proteins: Struct. Funct. Genet.* **5**, 183–201.
  51. Loh, S. N. & Markley, J. L. (1994). Hydrogen bonding in proteins as studied by amide hydrogen D/H fractionation factors: application to staphylococcal nuclease. *Biochemistry*, **33**, 1029–1036.
  52. Plaxco, K. W., Simons, K. T. & Baker, D. (1998). Contact order, transition state placement and the refolding rates of single domain proteins. *J. Mol. Biol.* **277**, 985–994.
  53. Myers, J. K. & Oas, T. G. (2001). Preorganized secondary structure as an important determinant of fast protein folding. *Nature Struct. Biol.* **8**, 552–558.
  54. Qiu, L., Pabit, S. A., Roitberg, A. E. & Hagen, S. J. (2002). Smaller and faster: the 20-residue Trp-cage protein folds in 4 micros. *J. Am. Chem. Soc.* **124**, 12952–12953.
  55. Mayor, U., Guydosh, N. R., Johnson, C. M.,

- Grossmann, J. G., Sato, S., Jas, G. S. *et al.* (2003). The complete folding pathway of a protein from nanoseconds to microseconds. *Nature*, **421**, 863–867.
56. Zhu, Y., Alonso, D. O., Maki, K., Huang, C. Y., Lahr, S. J., Daggett, V. *et al.* (2003). Ultrafast folding of alpha3D: a *de novo* designed three-helix bundle protein. *Proc. Natl Acad. Sci. USA*, **100**, 15486–15491.
57. Pace, C. N. (1986). Determination and analysis of urea and guanidine hydrochloride denaturation curves. *Methods Enzymol.* **131**, 266–280.
58. Royer, C. A., Hinck, A. P., Loh, S. N., Prehoda, K. E., Peng, X., Jonas, J. & Markley, J. L. (1993). Effects of amino acid substitutions on the pressure denaturation of staphylococcal nuclease as monitored by fluorescence and nuclear magnetic resonance spectroscopy. *Biochemistry*, **32**, 5222–5232.
59. Peterman, B. F. (1979). Measurement of the dead time of a fluorescence stopped-flow instrument. *Anal. Biochem.* **93**, 442–444.
60. Berberan-Santos, M. N. & Martinho, J. M. G. (1990). The integration of kinetic rate equations by matrix methods. *J. Chem. Educ.* **67**, 375–379.
61. Tanford, C. (1970). Protein denaturation. Part C. Theoretical models for the mechanism of denaturation. *Advan. Protein Chem.* **24**, 1–95.
62. Kraulis, P. J. (1991). MOLSCRIPT: a program to produce both detailed and schematic plots of protein structures. *J. Appl. Crystallog.* **24**, 946–950.
63. Wang, J., Truckses, D. M., Abildgaard, F., Dzakula, Z., Zolnai, Z. & Markley, J. L. (1997). Solution structures of staphylococcal nuclease from multidimensional, multinuclear NMR: nuclease-H124L and its ternary complex with Ca<sup>2+</sup> and thymidine-3',5'-bisphosphate. *J. Biomol. NMR*, **10**, 143–164.

*Edited by C. R. Matthews*

*(Received 2 October 2003; received in revised form 18 February 2004; accepted 19 February 2004)*